Air–Blood Barrier Translocation of Tracheally Instilled Gold Nanoparticles Inversely Depends on Particle Size

Wolfgang G. Kreyling,[†,‡,*] Stephanie Hirn,[†,#] Winfried Möller,[†] Carsten Schleh,[†,▽] Alexander Wenk,[†,⊗] Gülnaz Celik,[†,¶] Jens Lipka,[†] Martin Schäffler,[†] Nadine Haberl,[†,#] Blair D. Johnston,[†,◆] Ralph Sperling,[§,●] Günter Schmid,[⊥] Ulrich Simon,[∥] Wolfgang J. Parak,[§] and Manuela Semmler-Behnke[†,■]

[†]Institute of Lung Biology and Disease and [‡]Institute of Epidemiology II, Helmholtz Zentrum München — German Research Center for Environmental Health, 85764 Neuherberg/Munich, Germany, [§]Fachbereich Physik, Philipps Universität Marburg, 35037 Marburg, Germany, [⊥]Institute of Inorganic Chemistry, University Duisburg-Essen, 45141 Essen, Germany, and [∥]Institute of Inorganic Chemistry, RWTH Aachen University, 52056 Aachen, Germany. [#]Present address: Walter Brendel Centre of Experimental Medicine, Ludwig-Maximilians-University, 81377 Munich, Germany. [▽]Present address: Abteilung Gesundheitsschutz, Berufsgenossenschaft Holz and Metall, 81241 Munich, Germany. [⊗]Present address: Department of Infrastructure and Safety, Helmholtz Zentrum München, 85764 Neuherberg/Munich, Germany. [¶]Present address: Department of Chemistry, Industrial Biocatalysis, Technische Universität München (TUM), 85748 Garching, Germany. [◆]Present address: Adolphe Merkle Institute, Université de Fribourg, CH-1723 Marly 1, Switzerland. [●]Present address: Institut für Mikrotechnik, Johannes Gutenberg University of Mainz, Mainz, 55129 Mainz, Germany. [■]Present address: Bavarian Health and Food Safety Authority, 85764 Oberschleissheim, Germany.

ABSTRACT Gold nanoparticles (AuNP) provide many opportunities in imaging, diagnostics, and therapy in nanomedicine. For the assessment of AuNP biokinetics, we intratracheally instilled into rats a suite of ^{198}Au-radio-labeled monodisperse, well-characterized, negatively charged AuNP of five different sizes (1.4, 2.8, 5, 18, 80, 200 nm) and 2.8 nm AuNP with positive surface charges. At 1, 3, and 24 h, the biodistribution of the AuNP was quantitatively measured by gamma-spectrometry to be used for comprehensive risk assessment. Our study shows that as AuNP get smaller, they are more likely to cross the air–blood barrier (ABB) depending strongly on the inverse diameter d^{-1} of their gold core, *i.e.*, their specific surface area (SSA). So, 1.4 nm AuNP (highest SSA) translocated most, while 80 nm AuNP (lowest SSA) translocated least, but 200 nm particles did not follow the d^{-1} relation translocating significantly higher than 80 nm AuNP. However, relative to the AuNP that had crossed the ABB, their retention in most of the secondary organs and tissues was SSA-independent. Only renal filtration, retention in blood, and excretion *via* urine further declined with d^{-1} of AuNP core. Translocation of 5, 18, and 80 nm AuNP is virtually complete after 1 h, while 1.4 nm AuNP continue to translocate until 3 h. Translocation of negatively charged 2.8 nm AuNP was significantly higher than for positively charged 2.8 nm AuNP. Our study shows that translocation across the ABB and accumulation and retention in secondary organs and tissues are two distinct processes, both depending specifically on particle characteristics such as SSA and surface charge.

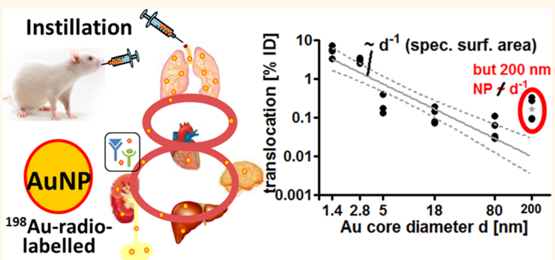

KEYWORDS: gold nanoparticles · ^{198}Au radiolabel · female Wystar–Kyoto rat · translocation · *in vivo* biodistribution · nanoparticle surface charge · specific surface area · intratracheal instillation

Gold nanoparticles (AuNP) continue to show a vast potential for applications in nanomedicine, yet much remains to be studied to gain a comprehensive understanding of how modified and unmodified AuNP interact with biological systems. AuNP show particular promise in the area of nanoscale drug-delivery systems and medical imaging[1,2] for many reasons, which have been recently reviewed.[3−5] As reported previously, AuNP possess high-tunability (*i.e.*, high control over shape, size, charge, and ligand composition), high stability (*i.e.*, low aggregation in case of appropriate surface coatings), high cell permeability, the ability to target the release of drug payloads (*i.e.*, through noncovalent drug loading using appropriate ligands or light- or glutathione-mediated release) and low apparent cytotoxicity. As such, AuNP and other metallic nanoparticles (NP) have been extensively tested in several studies related to drug delivery or tumor targeting.[6,7]

However, little is presently known about the properties of AuNP that determine their biokinetic fate. A very attractive target for local and systemic drug delivery are the lungs because of their large surface area

* Address correspondence to kreyling@helmholtz-muenchen.de.

Received for review June 26, 2013 and accepted December 23, 2013.

Published online December 23, 2013
10.1021/nn403256v

and close contact to the blood circulation.[8] The lungs are also likely to be a major route of occupational or environmental exposure to many engineered NP. Therefore, it is crucial to investigate the biokinetics of this uptake pathway to gain a better understanding of particle-related health risks.

AuNP are generally considered to have low toxicity, including in the pulmonary region.[9] However, toxicity both *in vivo* and *in vitro* has been noted under certain conditions. Previous researchers have shown no toxicity for either agglomerated or well-dispersed AuNP in rats.[10,11] Another recent study of different-sized AuNP indicated no genotoxic effects.[12] When using a triple cell coculture system, no changes in cell viability or cytokine release were observed, when exposed to AuNP.[13] In contrast, a few studies have determined that AuNP can show toxicity under certain conditions[14] such as cationic surface charge[15,16] or size considerations; *i.e.*, Chen and co-workers showed that intermediate sizes (8−37 nm) could cause toxic effects in mice after intraperitoneal administration;[17] see Alkilany and Murphy[18] and Khlebtsov and Dykman[19] for comprehensive reviews. In addition, cellular toxicity of 1.4 nm Au_{55} nanoclusters has been demonstrated,[20−22] which was attributed to their size (and, therefore, ease of crossing cellular and eventually nuclear membranes) and their ability to interact with ion channels and with the major groove of B-DNA.[21] Clearly, much still remains to be done in order to understand all of the potential mechanisms that may determine the toxicity of AuNP in clinical applications.

In terms of biokinetics and translocation, it appears likely that NP can cross the very thin air−blood barrier (ABB) to the circulation.[23] Indeed we and others have previously demonstrated that AuNP can cross the ABB.[5,24−26] Additionally, Patrick and Stirling have determined the biokinetic fate (up to 15 months) of radioactively ^{195}Au labeled citrate-stabilized 10−21 nm AuNP after a single microinjection into subpleural alveoli.[27] As in the present study, they also detected AuNP in several parts of the body 24 h postexposure. Moreover, they evaluated the fate of the AuNP in the lungs with transmission electron microscopy and detected agglomerated AuNP taken up by alveolar macrophages.[27] These findings are also in line with the results of Takenaka and co-workers, who showed agglomerated AuNP of 20 nm size taken up by alveolar macrophages in rat lungs 24 h after inhalation.[28,29] In addition, our recent inhalation study using 20 nm AuNP shows that only a low percentage of the AuNP could be found in alveolar macrophages in bronchoalveolar lavages from the exposed mouse lungs 24 h postexposure.[30] The translocation of NP across the ABB is not yet fully understood, but there is strong evidence that transcellular routes are mainly responsible for NP translocation while paracellular transport plays a minor role under normal circumstances.[31] Semmler-Behnke and co-workers[32] have shown that along with initially limited phagocytosis by alveolar-macrophages, a rapid translocation of inhaled 20 nm iridium NP into the lung epithelium and interstitium takes place and persists during the entire retention time of six months.

Nevertheless, long-term clearance seems to be maintained by alveolar macrophage-mediated transport from the interstitium and the bronchial-associated-lymph-nodes (BALT) onto the epithelium and *via* the mucociliary escalator of the airways to the larynx.[32,33] However, several intracellular entry routes (endocytosis), transport and exocytosis processes for this behavior seem to depend on the size and other parameters of AuNP, but a detailed picture of these transport processes is still largely unclear, and more work is required in this area.[34,35]

In this present study, we continue to study the *in vivo* biokinetics of AuNP by evaluating the biodistribution of monodisperse, spherical AuNP of different core sizes with well-defined surface ligands of different surface charges, at various time points up to 24 h following intratracheal instillation. Admittedly, the AuNP suspension instillation is less physiological and delivers the AuNP at a rather high dose rate compared to an inhalation exposure. Yet, it is a currently well accepted methodology in nanotoxicology that allows for rather precise dosing and confers the ability to study a large number of rodents, in numerous treatment groups, using six different AuNP, at three different time points. The current work completes a series of experimental studies to determine the 24 h biokinetics of the same set of AuNP after different routes of administration: (1) systemic administration *via* intravenous injection for examination of the direct accumulation and retention from blood circulation into organs and tissues,[36] (2) oral ingestion *via* intraesophageal instillation for investigating the absorption through the intestinal wall,[37] and now in this study (3) lung exposure *via* intratracheal instillation for the measurement of the passage through the ABB with the intention to ascertain which NP characteristics are the primary determinants of AuNP translocation through the ABB into the blood circulation. The main aim of this study is to determine the translocation of AuNP as a function of particle size. We measure the amount of gold (expressed in radioactivity, *i.e.*, proportional to the mass of gold (Au)) that has been accumulated and retained in various organs and tissues of the body after a specific time. Furthermore, our study suggests to find a predictive parameter that is general and that can in principle be applied to any shape of nanoparticles, *e.g.*, to anisotropic particles such as rods or wires, where particle size is not a predictive parameter. This, however, needs to be demonstrated in future studies. Hence, by looking for descriptive parameters of AuNP cores, we observed that translocation across the ABB is inversely proportional to the AuNP core diameter

TABLE 1. Physicochemical Parameters and Dose Metrics of Administered ^{198}AuNP and Their Radioactive Labels; Additionally Dose Metrics of ^{198}Au

AuNP, Au core diameter (nm)	1.4	5	18	80	200	2.8	2.8
surface modification/ligand	S-TPP (SO_3^-)[53]	S-TPP (SO_3^-)[39]	S-TPP (SO_3^-)[53]	S-TPP (SO_3^-)[39]	S-TPP (SO_3^-)[39]	TGA (COO^-)[38]	CA (NH_3^+)[38]
hydrodynamic diameter (nm)	2.9[a]	12.1[c]	21[c]	85[b]	205[b]	ND[d,f]	ND[d,f]
polydispersity index (PdI)	ND[f]	0.19	0.10	0.12	0.05	ND[d,f]	ND[d,f]
pH value of suspension	5.6	5.8	6.4	5.4	5.5	ND[f]	ND[f]
zeta potential (mV)	-20.6 ± 0.5	-21.1 ± 1.4	-22.8 ± 3.1	-22.3 ± 1.6	-41.3 ± 4.5	negative	positive
charges per AuNP (calculated)[e]	12	88	952	17721	109607	115	115
specific ^{198}Au radioactivity (GBq/g)	72	6.7	31	14.9	11.5	15.8	5.5
isotope ratio of ^{198}Au to stable ^{197}Au	8.0×10^{-6}	7.4×10^{-7}	3.4×10^{-6}	1.7×1^{-6}	1.3×10^{-6}	1.7×10^{-6}	6.1×10^{-7}
ratio of ^{198}Au per NP	6.6×10^{-4}	2.8×10^{-3}	0.60	26	307	1.2×10^{-3}	4.1×10^{-4}
admin ^{198}Au radioactivity (kBq) per rat	188 ± 27	163.9 ± 9.7	78.5 ± 6.6	263.0 ± 8.6	162.1 ± 24.2	12.2 ± 1.3	107.6 ± 7.5
admin mass of gold NP (μg) per rat	2.6 ± 0.4	34.5 ± 2.0	2.5 ± 0.2	17.6 ± 0.6	14.1 ± 2.1	0.8 ± 0.1	19.5 ± 1.4
admin number of gold NP per rat	$9.5 \pm 1.4 \times 10^{13}$	$2.8 \pm 0.2 \times 10^{13}$	$4.4 \pm 0.4 \times 10^{10}$	$3.5 \pm 0.1 \times 10^{9}$	$1.8 \pm 0.3 \times 10^{8}$	$3.6 \pm 0.4 \times 10^{12}$	$8.9 \pm 0.6 \times 10^{13}$
admin surface area (cm^2)	$5.8 \pm 0.9 \times 10^{\circ}$	$2.2 \pm 0.1 \times 10^{1}$	$4.5 \pm 0.4 \times 10^{-1}$	$7.0 \pm 0.2 \times 10^{-1}$	$5.6 \pm 0.8 \times 10^{-1}$	$7.0 \pm 0.7 \times 10^{-1}$	$1.8 \pm 0.1 \times 10^{1}$
admin specific surface area (m^2/g)	$2.3 \pm 0.04 \times 10^{-1}$	$6.3 \pm 0.2 \times 10^{-2}$	$1.8 \pm 0.02 \times 10^{-2}$	$3.9 \pm 0.6 \times 10^{-3}$	$1.6 \pm 2.1 \times 10^{-3}$	$9.0 \pm 0.1 \times 10^{-2}$	$9.0 \pm 0.1 \times 10^{-2}$

[a] As determined earlier[57,58] [b] Dynamic light scattering (DLS) measurement using Malvern HPPS5001, Herrenberg, Germany; in addition: TEM and UV−vis analyses confirmed the core size of the AuNP.[46] [c] DLS measurement using Malvern Zetasizer Nano ZS, Herrenberg, Germany. [d] Hydrodynamic diameter and PdI were not determined, but the mean core size ± SD of both batches of AuNP already surface modified with either the carboxyl or the amino groups were determined to be 2.8 ± 0.4 nm. [e] Size and orientation of the surface molecules were used for the estimated number of molecules on the AuNP surface. [f] ND: not determined.

between 1.4 and 80 nm but not for 200 nm AuNP. This parameter d^{-1} happens to be proportional to the ratio of surface area over volume of these spheres, *i.e.*, their specific surface area SSA. This linear relation is only valid for the entire translocation across the ABB. This relation proportional to the inverse diameter d^{-1} also holds when considering translocation from the lungs relative to the administered AuNP dose, including uptake in most of the secondary organs and tissues. However, when relating the accumulated AuNP in organs and tissues to the percentage of AuNP that had crossed the ABB, this trend was largely lost as no size dependency of AuNP could be seen. Both findings are novel and have not been reported in the open literature yet. This linear proportionality is biologically plausible since smaller NP have a higher probability to cross the ABB compared to larger NP. Note, the linear relation is a novel observation, and it is a rather simple relation when considering the complexity of the transport of the AuNP, which we will discuss later. In addition, we emphasize that we distinguish AuNP translocation across the ABB *versus* AuNP accumulation and retention from blood to the various organs and tissues as separate steps, which may not both follow the same AuNP dependencies.

RESULTS AND DISCUSSION

AuNP Characterization. Negatively charged AuNP of 1.4, 5, 18, 80, 200 nm Au core diameter were obtained after surface modification using sulfonated triphenylphosphine (S-TPP, SO_3^-).[38,39] Negatively charged 2.8 nm AuNP were generated by substituting the original ligand triphenylphosphine by thioglycolic acid (TGA, terminal group COO^-), whereas positively charged 2.8 nm AuNP were generated by substituting the original ligand TPP by cysteamine equipped with positively charged NH_3^+ groups. Physicochemical parameters of all AuNP including core and hydrodynamic diameters are given in Table 1; more details about the measurements are given in the Supporting Information and have been assessed previously.[36,37] In this work the experimental results of AuNP retention and translocation are given in percent (wt) of the initial AuNP dose delivered to the peripheral lungs (% ID), as described in detail in the Methods section. Note, all the stated AuNP percentages represent exclusive AuNP retention in the organs/tissues without the AuNP fraction in the blood volume of these organs/tissues (see Methods). Furthermore, the AuNP fraction being cleared by mucociliary transport into the gastrointestinal tract (GIT) and feces was excluded from balanced calculations to obtain the percentage of the retained AuNP in the lungs as the primary organ or being translocated to secondary organs and tissues (see Methods). For correlation analysis between particle size and biokinetics we focused on the diameter of the AuNP core that was determined by TEM. The Au core diameter proved to be more suitable for our correlation estimates compared to the hydrodynamic diameter of the administered AuNP, which may only be valid at the time of administration, but may be rapidly modified by protein absorption in the lung lining fluid.[40] In the latter review, the difference between the Au core diameter and the more variable hydrodynamic diameter are discussed. Yet, we are aware that molecular interactions with cells and body fluids occur on the surface of the AuNP and their protein corona.[37,41,42] Therefore, we used only negative ionic S-TPP surface ligands as an initial step of standardization. When using positive *versus* negative ionic ligands we found significant differences in the biokinetics of same-sized 2.8 nm AuNP, underlining the importance of initial surface modification on the subsequent formation of the protein corona *in vivo*.

Since we detected the organ-retained AuNP fractions only by their radioactive properties, we cannot discriminate between particle, atomic zerovalent Au° and ionic (dissolved) Au as a result of AuNP degradation and dissociation. As discussed in a recent review by Brown and co-workers such degradation and dissociation cannot be excluded in biological systems.[9] Yet, this always leads to the formation of both atomic Au° and ionic Au^{3+} in parallel. In order to study the biodistribution of ionic Au^{3+}, we intratracheally instilled soluble Au^{3+} ions in $HAuCl_4$ solution radioactively labeled with ^{198}Au and determined the 24-h biodistribution (see Methods). The results are shown in Table S2 and discussed in Supporting Information. These data show that the entire Au ion biodistribution is completely different from that of the AuNP. As determined in the Supporting Information, conservative estimates show that potentially dissolved Au remains to be negligibly low in the lungs and below a few percent of the Au retention in secondary organs and in the carcass. Hence, we cannot completely exclude the dissolution of AuNP. But according to the additional biodistribution study using soluble Au ions and our estimates on potentially dissolved Au retentions, dissolution only modestly modifies AuNP retention in all organs and tissues. Hence, these additional data confirm our findings on translocation across the ABB and subsequent accumulation and retention of AuNP in secondary organs and tissues.

AuNP Retention in the Peripheral Lungs. The mucociliary-cleared AuNP fraction at 24 h was between 20 and 50% of the initially delivered AuNP dose and showed a rather large variation between individual animals as well as for different sizes of AuNP (Table S1, Supporting Information). There was no significant trend of MCC with particle size, which is similar to the findings of Patrick and Stirling.[43] This variability is intrinsic to intratracheal instillation and it is well-known. We tried to reduce this variability by (a) applying the instillation during the inspiration of the spontaneously breathing rat and (b) the instillation procedure was performed by only one experienced person of our team.

After correcting for the rapidly cleared NP fraction from the airways by mucociliary action (MCC) the 24 h AuNP retention in the peripheral lungs was least for the smallest AuNP (1.4 nm) (Figure 1; see also ref 5). The retention increased for the 2.8 nm COO^- AuNP and was even higher for the 5 nm AuNP (as previously shown[26]). For the larger AuNP, 24 h lung-retention increased further and ranged between 99.8 and 99.9% (Figure 1).

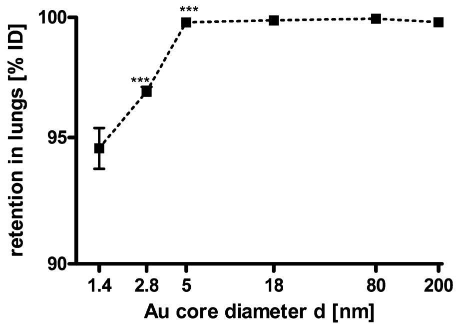

Figure 1. Lung retention 24 h after intratracheal instillation of negatively charged, spherical, monodisperse AuNP (1.4, 5, 18, 80, 200 nm Au core diameter coated with S-TPP and 2.8 nm Au core diameter carboxyl-coated); AuNP percentages of the initial dose delivered to the peripheral lungs (ID). Note, scale is in log for *x*-axis. Data are mean ± SEM, *n* = 4 rats. Significant changes in retention of given AuNP sizes *versus* those of the next smallest size are indicated, as determined by the ANOVA with posthoc Tukey test. (* $p < 0.001$).**

Size and Time-Dependent Translocation of AuNP across the ABB. Our study shows, as AuNP get smaller they are more likely to cross the ABB. This is shown in Figure 2A, where the total 24 h translocation across the ABB of the AuNP increases with decreasing Au core diameter between 1.4 and 80 nm. This increase follows a trend proportional to the inverse diameter d^{-1} of the Au core. According to the following equation, the proportionality to d^{-1} corresponds to the specific surface area (SSA) of these spherical AuNP:

$$SSA = \frac{SA}{m} = \frac{SA}{\rho V} = \frac{\pi d^2}{\rho d^3} = \frac{6}{\rho d} \sim \frac{1}{d} \qquad (1)$$

where d = AuNP diameter, $m = \rho V$ = AuNP mass, ρ = AuNP density, SA = πd^2 = AuNP surface area, $V = \pi/6d^3$ = AuNP volume.

In Figure 2A, the trend proportional to the inverse diameter d^{-1} or according to SSA is shown together with data from each individual rat. Note, to our knowledge such an AuNP-SSA-dependent *in vivo* translocation over the full nano size range of 1.4–80 nm NP has not yet been described and requires further research on the mechanistic side. Note, the d^{-1} dependence is an unexpected and, at the same time, a remarkably simple relation when considering the complexity of AuNP transport across biological barriers, involving several steps: (1) predominantly through and/or possibly in between epithelial cells, (2) through the interstitial space, and (3) across the vascular endothelium to finally reach the blood circulation.

Since particle diffusion also increases with the inverse diameter d^{-1}, passive particle diffusion would

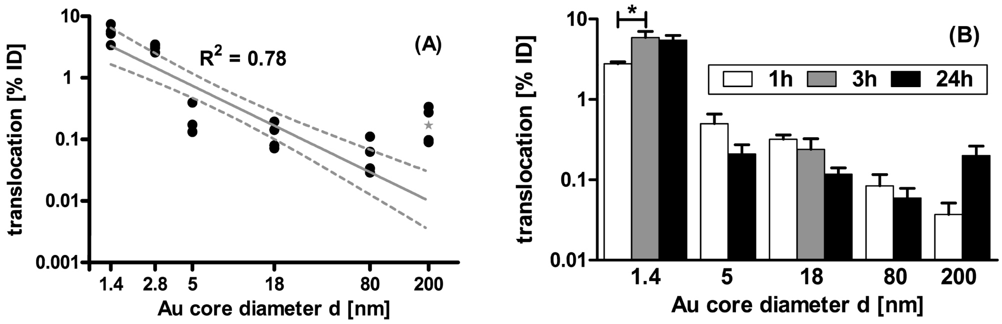

Figure 2. (A) Percentages of 24 h translocation of intratracheally instilled AuNP *versus* the Au core diameter *d*. Note, data are normalized to the initial dose delivered to the peripheral lungs (ID). Data are from individual rats ($n = 4$) on a double-log scale. Negatively charged, spherical AuNP (1.4, 5, 18, 80, 200 nm Au core diameter coated with S-TPP; 2.8 nm carboxyl-coated) were used. Significant changes of translocation of the mean of given AuNP sizes *versus* those of next smallest size are indicated, as determined by the ANOVA with posthoc Tukey test (* $p < 0.001$). The power law-trend $\sim d^{-1}$ (exponent was -1.16; 95% confidence interval (-0.86, -1.47), $p < 0.001$, coefficient of correlation $R^2 = 0.78$) is the best fit of the data from 1.4 to 80 nm AuNP and is equivalent to the SSA of AuNP. The dashed lines of the confidence interval were calculated for 1.4–80 nm AuNP and extrapolated to 200 nm AuNP. The mean measured translocation for the 200 nm AuNP is significantly larger than the estimated extrapolation data ($p > 0.05$), indicating a different behavior of the 200 nm AuNP compared to all smaller AuNP. (B) Percentages of translocation of intratracheally instilled, negatively charged, spherical AuNP (1.4, 5, 18, 80, 200 nm Au core diameter coated with S-TPP) after 1, 3, and 24 h. Data are normalized to the initial dose delivered to the peripheral lungs (ID). Data are mean $\pm$ SEM, $n = 4$ rats. Significant changes of translocation between the different time points for each AuNP size are indicated as determined by the ANOVA with posthoc Tukey test (* $p < 0.05$).**

be the simplest explanation for our results from a pure physical point of view. Particle diffusion is a passive, thermodynamic process only driven by thermal energy kT, which does not involve any active transport, including receptor mediated uptake and release, as illustrated above. Although we believe that passive diffusion will be a too simplistic picture to explain the observed translocation regarding the complexity of translocation processes across the ABB, it may serve suitable for simulations. Since our data follow the inverse-diameter-dependent-law, this may represent a general expression incorporating all the above-mentioned active processes, and may also be useful for testing new hypotheses of particle translocation across the ABB.[44]

Surprisingly, the 200 nm AuNP did not follow this trend, and in comparison to the 80 nm AuNP a much higher percentage of translocated particles was found. Actually, the translocation of the 200 nm gold particles was similar to that of the 5 nm AuNP. Yet, disintegration of these solid gold spheres can be excluded. Extrapolating the trend proportional to the SSA toward 200 nm gold particles, and including the statistical confidence interval, the extrapolated data are significantly lower than those observed for the 200 nm AuNP (Figure 2A). Hence, the 200 nm AuNP do not follow the translocation of nanoscale particles according to their SSA suggesting that different translocation mechanisms may underlie 200 nm AuNP translocation across the ABB, compared to nanosized AuNP. For instance, Rejman and co-workers[45] have reported caveolae-mediated endocytosis of particles >200 nm *versus* clathrin-mediated endocytosis of <200 nm particles. The increased *in vivo* translocation of 200 nm gold particles across the ABB compared to the AuNP-SSA dependent translocation may result from different endocytotic and/or exocytotic processes or, less likely, from passive diffusion-type processes; this requires more mechanistic studies.

We have also investigated the time-dependent biokinetics for the five different sized S-TPP coated AuNP between 1 and 24 h, with additional 3 h data for 1.4 and 18 nm AuNP. The total translocated AuNP percentage is shown in Figure 2B for all five AuNP sizes, indicating that the translocation of 5, 18, and 80 nm AuNP is virtually complete after 1 h, and there is even a nonsignificant decreasing trend after 24 h. However, for 1.4 nm AuNP translocation continues to increase until 3 h after instillation with no further change thereafter. The underlying mechanisms remain unclear, although it appears plausible that the very small 1.4 nm may remain more mobile for a longer time interval while crossing the ABB with its different cell types when compared to the larger-sized AuNP. Interestingly, after 1 h the translocation of 200 nm AuNP is lower than those of all nanoscaled AuNP and follows the same decreasing trend with increasing AuNP diameter. However, the 24 h translocation of 200 nm AuNP is strongly increased compared to the 1 h translocation, indicating prolonged translocation across the ABB that occurs only for 200 nm AuNP but not for the smaller nanoscale AuNP. The mechanisms for prolonged translocation remain unclear since no other kinetic data on the various steps of translocation across the ABB are available for different sizes of AuNP. Yet, we have observed prolonged translocation across the rat ABB during the first week after inhalation of 20 nm iridium NP as well.[46] This may indicate that physicochemical properties of the NP are important determinants. The occurrence of prolonged translocation after

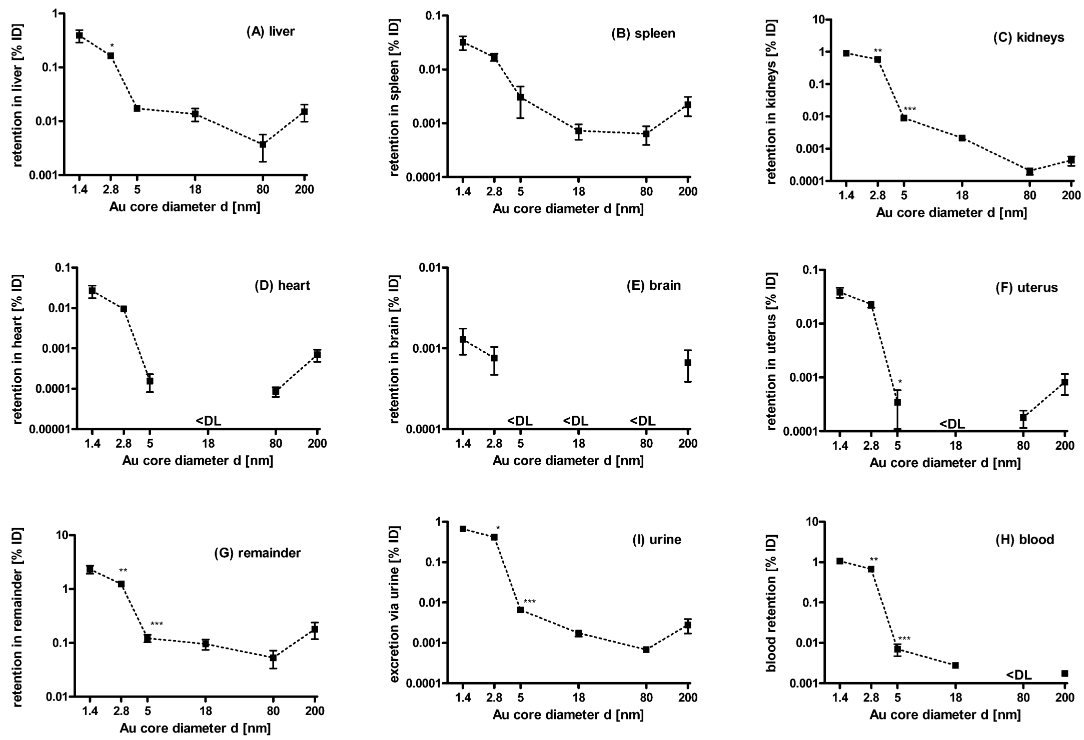

Figure 3. AuNP retention 24 h after intratracheal instillation of negatively charged, spherical, monodisperse AuNP (1.4, 5, 18, 80, 200 nm Au core diameter coated with S-TPP; 2.8 nm carboxyl-coated). AuNP percentages of initial dose delivered to the peripheral lungs (ID) are given for each of whole secondary organs in separate panels, as well as the entire remaining carcass (remainder, panel G) and total blood and urine; in each panel the respective organ, tissue, or body fluid is indicated. Data are mean $\pm$ SEM, $n = 4$ rats. Note, scale is double-log. Significant changes of retention of given AuNP sizes *versus* those of next smaller size are indicated, as determined by the ANOVA with posthoc Tukey test (* $p < 0.05$, ** $p < 0.01$, *** $p < 0.001$). (<DL: lower than detection limit).

inhalation of iridium NP supports our current findings on AuNP.

AuNP Organ and Tissue Biodistribution and Retention during the First 24 h. First, we show the AuNP biodistribution in secondary organs, tissues, and body fluids using conventional data normalization to the initial AuNP dose in the peripheral lungs (ID). In a second more interesting step, the same data are shown relative to the AuNP amount that had crossed the ABB and was circulating in blood, for subsequent accumulation and retention in secondary organs and tissues.

Our results show a strong size-dependency of the accumulation and retention of AuNP in all organs, tissues, and urine after 24 h relative to the initial AuNP dose delivered to the peripheral lungs (Figure 3). AuNP percentages per weight (in gram) of organ/tissue are given in Table S3, Supporting Information. Similar to total translocation, as shown in Figure 2, organ and tissue retention of the smallest AuNP is highest and declining until 80 nm AuNP. Regarding the biodistribution, AuNP retention in the remaining carcass (consisting of skeleton, soft tissue and fat) was higher than in all secondary organs and body fluids for all AuNP sizes used (Figure 3G). This high retention in the carcass is an important new observation grossly neglected in the current literature. Even more important is the fact that between 10 and 20% of the carcass retention was found in the skeleton as we showed previously for two different inhaled iridium NP (20 nm and 80 nm) and elemental carbon NP (25 nm).[47] Since the NP must have entered the skeleton *via* blood circulation it is most likely that the NP are retained in the bone marrow directly in the vicinity of pluripotent stem cells, which are considered to be most sensitive to exogenous material. Comparing AuNP retention in secondary organs, 1.4 nm S-TPP AuNP and 2.8 nm COO^- AuNP retention in kidneys was highest, even significantly higher than for liver, where the highest retention was expected. For the larger AuNP, liver retention was higher than for kidneys (Figure 3A+C). Also the 1.4 nm S-TPP AuNP and 2.8 nm COO^- AuNP retention in blood and urine ranked similarly to retention in kidneys and was higher than for all other organs (Figure 3).

In the following, we consider the biokinetics during 24 h in individual organs and tissues for the five different-sized, S-TPP coated AuNP from 1 to 24 h with additional 3 h data for 1.4 and 18 nm AuNP. Similar to totally translocated percentages of AuNP already mentioned above, there is an increase in the retention of 1.4 nm AuNP in several organs and tissues from 1 to 24 h (Figure S1, Supporting Information). For 5 nm AuNP, the retention increases from 1 to 24 h in liver, spleen, heart, and kidneys is largely compensated by the decrease in the remaining carcass. For 18 and

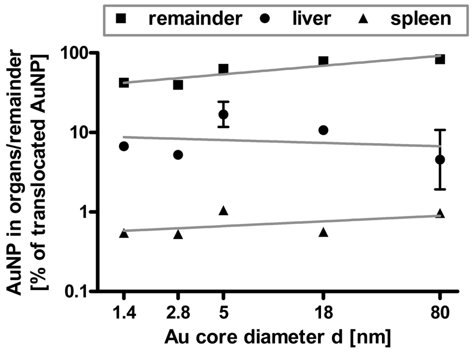

Figure 4. Percentages of translocated AuNP in remainder, liver, and spleen 24 h after intratracheal instillation. Note, AuNP retention was not normalized to initial lung dose but to the total of translocated AuNP; note, the scale is double-log. Data are mean ± SEM, $n = 4$ rats. Negatively charged, spherical AuNP (1.4, 5, 18, 80 nm Au core diameter, coated with S-TPP; 2.8 nm carboxyl-coated); gray lines are linear trend lines and indicate no significant dependence on AuNP diameter.

80 nm AuNP 1 and 24 h retention of most organs and the remaining carcass are similar, indicating complete translocation already 1 h after intratracheal instillation. Hence, not only is translocation across the ABB higher for 1.4 and 5 nm AuNP but also their translocation, accumulation, and retention in secondary organs last longer than for the larger AuNP. Note, translocation and retention of 200 nm AuNP are also prolonged over 24 h in liver and spleen, which leads to higher total translocation than those of 18 and 80 nm AuNP.

AuNP Biodistribution Relative to the Amount of Translocated AuNP. When normalizing the accumulated AuNP percentages in each secondary organ or tissue to the percentage of total translocated AuNP across the ABB, the retention of AuNP appears to be size-independent for the remainder, liver, spleen, brain, and uterus (Figure 4). The uptake by resident macrophages plays an especially important role for liver and spleen. The data suggest that these AuNP are obviously taken up in these organs independently of size or SSA, which is likely due to the slow blood flow through the rather small, "leaky" sinusoidal capillaries with macrophages residing on their walls, as we and others showed earlier.[36,48]

Comparing these results with those obtained from a previous study of intravenous injection of the same suite of AuNP as used in the present study, it is most striking that the pattern in liver is completely different between intravenously injected AuNP and those translocated through the ABB into circulation after intratracheal instillation.[36] Following intravenous injection the AuNP retention in the liver was almost 100% for all large AuNP ≥ 18 nm; for smaller AuNP it was declining and for the smallest AuNP (1.4 nm) it was about 50% of the ID to the peripheral lungs. In our present study, it is completely opposite: liver retention is AuNP-size-independent, varying slightly below 10% of the translocated AuNP fraction (Figure 4). Similarly, the size-dependent patterns found in all other secondary organs (except kidneys; see below) and the remainder, after intravenous injection, were not observed in the present study. This significant difference in the AuNP biodistribution obtained after two different routes of AuNP administration to circulation indicates major differences in the pathways of AuNP processing in the organism. This issue will be discussed more closely in a future manuscript. The rapid accumulation of AuNP in the liver after IV injection may well be triggered by a predominant albumin corona, while the protein corona of the AuNP that translocated first through the ABB may be more complex and may contain more proteins of less abundance but higher affinity. Similarly, the lower accumulation and retention in the liver gives rise to more accumulation in other secondary organs and tissues. It is also remarkable that AuNP content in blood 24 h after IV injection is much greater (Figure 1H in our previous paper[36]) than that of AuNP that had crossed the ABB.

The possible role of major AuNP agglomeration in circulation can grossly be excluded, since we observe SSA-dependent biodistribution in both *in vivo* AuNP studies, either after intratracheal instillation or intravenous injection. Hence, we hypothesize the major differences in biodistribution are predominantly caused by surface modification and protein binding after deposition in the lungs. AuNP surface modification during the prolonged and complex process of ABB translocation may differ strongly from serum protein interaction of intravenously injected AuNP in the circulation. As highlighted above and in the Supporting Information, possible particle dissolution cannot completely be excluded but may play only a minor role in our AuNP biodistribution studies.

Interestingly, both, the AuNP retention in blood and the retention in kidneys (relative to the total translocated AuNP) are size-dependent. As indicated in Figure 5 this trend is also close to the inverse diameter d^{-1} (which represents the SSA dependency of AuNP; see eq 1). Yet, the trend found for urinary excretion was closer to $d^{-0.5}$. Note, the d^{-1} dependency of the retention in kidneys relative to the translocated AuNP is an independent observation from the kidney retention shown in Figure 3C, in which the kidney percentage is given relative to the administered ID. However, after intravenous injection of the same AuNP, the retention in kidneys was not SSA-dependent but showed an inverse size-dependency only for small AuNP (≤18 nm) and no size-dependency for larger AuNP.[36]

It has been described recently that molecular structures smaller than 50 kDa (including NP below a hydrodynamic diameter of 5.5 nm) are almost quantitatively cleared by the kidneys into the urine. This was shown for 1.9 nm AuNP of undisclosed surface

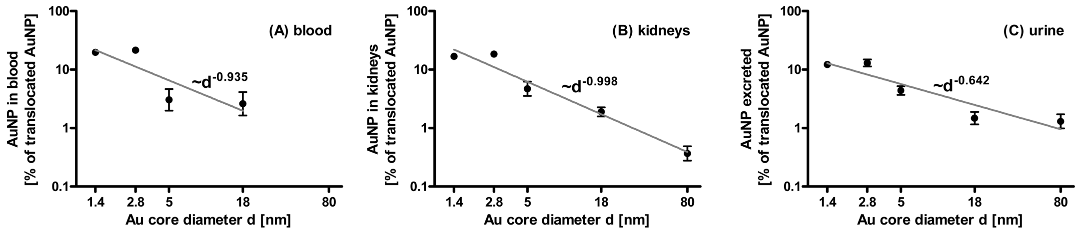

Figure 5. Percentages of translocated negatively charged, spherical AuNP (1.4 nm, 5 nm, 18 nm, 80 nm Au core diameter coated with S-TPP; 2.8 nm carboxyl-coated) in blood, kidneys, and urine 24 h after intratracheal instillation. Note, AuNP retention was not normalized to initial lung dose but the total translocated fraction; note, the scale is double-log. Data are mean ± SEM, n = 4 rats. Gray lines illustrate particle size-dependent linear trends proportional to d^{exp}, which is particularly close to d^{-1} in kidneys and blood, *i.e.*, proportional to AuNP specific surface area (SSA); regression coefficients: $R^2_{blood} = 0.57$, $R^2_{kidneys} = 0.91$, $R^2_{urine} = 0.79$.

modification being used as an X-ray contrast agent[2] and for quantum dots (QD) with a zwitterionic surface coating.[49] The surface modifications of both NP were described to prevent protein binding. In fact, serum protein binding was shown to lead to a substantial growth of NP size when the QD were coated with charged molecules.[49] Since we did not find such a high urinary excretion rate as those of QD < 5.5 nm and AuNP of 1.9 nm,[2,49] we hypothesize that protein binding may be an important factor for our AuNP, being responsible for both the increased retention of the 1.4, 2.8, and 5 nm AuNP in the body, and for lower urinary excretion. There is evidence that S-TPP coating of the AuNP (same as we used in this study) can be substituted or detached in biological media.[20] Therefore, we hypothesize that S-TPP coating may be replaced by proteins of the various body fluids. These proteins that are bound to the surface of the AuNP are likely to increase their overall size, as we showed in an *in vitro* study using same-sized AuNP.[50] Since the glomerular filtration threshold in kidneys is believed to be 7−9 nm,[48] it appears plausible that about 15% of the AuNP-protein-conjugates of the originally 1.4 and 2.8 nm AuNP are small enough to be able to pass through the very thin basal membrane to be excreted *via* urine. It needs to be noted that proteins seem to have a high impact on the biodistribution of NP and also influence glomerular filtration in kidneys.[51]

Yet, we found SSA-dependent renal filtration of AuNP from blood into urine as demonstrated by the decreasing retention with increasing size of AuNP (1.4−80 nm) (Figure 5). The blood pressure forces fluid from the capillaries of the glomerulus through the epithelial layer of the Bowman capsula into the lumina of the proximal tubulus. The exact structure is still under debate, but Rodewald and co-workers[52] have already suggested that the glomerular barrier is built by three layers, which a molecule or NP needs to cross: (a) the fenestrated capillary endothelium (diameter: 50−100 nm), (b) the basement membrane, and (c) the slit diaphragm built by epithelial podocytes (diameter: 7−14 nm). The glomerular barrier may likely play a predominant role in the size-dependent clearance pattern we observed.[53] Furthermore, our data suggest that even AuNP larger than 5 nm are excreted *via* urine even though those urinary AuNP fractions are rapidly declining with size.

Effect of Surface Charge of Carboxylated *versus* Aminated 2.8 nm AuNP. After 24 h, most of the applied AuNP (either negatively or positively charged) were found in the lungs; they were significantly higher for 2.8 nm NH_3^+ AuNP than for 2.8 nm COO^- AuNP, 98.8 and 96.6%, respectively. Accordingly, the translocated AuNP percentage, relative to initial dose of the peripheral lungs, is higher for the negative AuNP than for the positive AuNP (Figure 6A). Recent studies showed that the surface-charge played an important role for the uptake efficiency in cells.[54] Our data suggest that the surface-charge of AuNP also modulates translocation and accumulation and retention in secondary organs; *i.e.*, negatively charged AuNP translocated significantly more to blood than positively charged AuNP and accumulated more in secondary organs and tissues than positively charged 2.8 nm AuNP (Figure 6B).[16] Translocation into blood implies crossing membranes, which can be either paracellular or transcellular. The last of both mechanisms covers uptake and release (exocytosis) of particles, and because previous studies have shown higher uptake of positively compared to negatively charged particles,[35] less efficient release may be one simple explanation for reduced translocation of the positively charged particles. Accounting only the amount of AuNP that crossed the ABB, the AuNP accumulation and retention was the same for both charges in each secondary organ (Figure 6C). Interestingly, there are major differences when compared to the intravenously injected AuNP of our previous study.[36] For correct comparison, we need to compare the retained AuNP percentages relative to the AuNP amount that had crossed the ABB. In contrast to our present data where we found dominant retention in the kidneys (∼20%), carcass (∼40%), blood (∼20%), and also in urinary excretion (∼14%) and only about 5% in liver of both charged 2.8 nm AuNP after IV injection, more than 70% were retained in the liver followed by about 10% in spleen and carcass and very

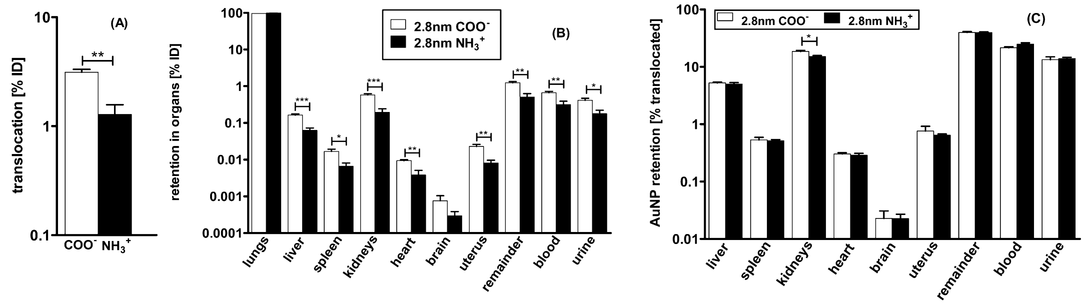

Figure 6. (A) Percentages of negatively and positively charged 2.8 nm AuNP translocated across the ABB during 24 h postexposure, relative to ID. Translocation is given in log scale. Data are mean ± SEM, $n = 4$ rats. Significant changes between the 2.8 nm COO^- and 2.8 nm NH_3^+ AuNP are indicated, as determined by the student's t test (** $p < 0.01$,). (B) Percentages of translocated AuNP (2.8 nm Au core diameter, carboxyl- or amino-coated) in secondary organs, tissue, remainder, blood, and urine 24 h after intratracheal instillation, relative to ID. Percentages are given in log-scale. Data are mean ± SEM, $n = 4$ rats. Significant changes between the 2.8 nm COO^- and 2.8 nm NH_3^+ AuNP are indicated as determined by the student's t test (* $p < 0.05$, ** $p < 0.01$, *** $p < 0.001$). (C) Percentages of translocated AuNP (2.8 nm Au core diameter, carboxyl- or amino-coated) in secondary organs, tissue, remainder, blood, and urine 24 h after intratracheal instillation, relative to the amount of AuNP which had translocated the ABB. Percentages are given in log-scale. Data are mean ± SEM, $n = 4$ rats. Significant changes between the 2.8 nm COO^- and 2.8 nm NH_3^+ AuNP are indicated, as determined by the student's t test (* $p < 0.05$).

low percentages in all other secondary organs. In addition, in the previous intravenous study, there were significant retention differences between the differently charged 2.8 nm AuNP, not only in kidneys but also in liver, spleen, heart, and the remaining carcass. These findings strongly suggest that the protein corona of AuNP formed in blood differed strongly after the different application pathways of intravenous injection and intratracheal instillation and subsequent translocation across the ABB.

In addition, this finding may be related to the fact that positively and negatively charged NP may bind different proteins maintaining their different biokinetic fate and uptake in kidneys. As the glomerular basement membrane is negatively charged, there might be a different filtration rate for differently charged molecules, but this issue is still under debate.[55]

CONCLUSION

The present study describes the influence of physicochemical properties of intratracheally instilled AuNP on their biokinetics. AuNP properties, such as the size and SSA of the spherical Au core and surface charge, affect their translocation across the ABB, their organ retention, and also their renal clearance rate. Importantly, essential AuNP properties seem to be changed after crossing the ABB, since the biokinetics depended on the SSA of the AuNP, while the retention of most secondary organs (except kidneys) was independent of SSA. The latter size dependency was different in comparison to the AuNP retention after a direct intravenous administration. The underlying mechanisms are still unclear, but an impact of a modified protein binding is very likely.

METHODS

Animals. A total of 60 healthy, female Wistar−Kyoto rats (WKY/Kyo@Rj rats, Janvier, Le Genest Saint Isle, France), 8−10 weeks old (approximately 250 g body weight) were housed in pairs in humidity- and temperature-controlled ventilated cages on a 12 h day/night cycle prior to the experiments (4 rats per treatment group). A rodent diet and water were provided *ad libitum*. All experiments were conducted under German Federal guidelines for the use and care of laboratory animals and were approved by the Regierung von Oberbayern (Government of District of Upper Bavaria Approval No. 211−2531−94/04) and by the Institutional Animal Care and Use Committee of the Helmholtz Center Munich.

AuNP Preparation and Characterization. We used the same panel of AuNP as were already used for biokinetic studies following intravenous injection[36] and gavage.[37] As previously described, AuNP surfaces were modified yielding negative or positive surface charges using sulfonated triphenylphosphine (S-TPP, SO_3^-); see also the preparation in the Supporting Information.[38,39] In addition, negatively charged 2.8 nm AuNP were generated by substituting the original ligand S-TPP by thioglycolic acid (TGA, terminal group COO^-), whereas positively charged 2.8 nm AuNP were generated by substituting the original ligand S-TPP by cysteamine (CA, terminal group NH_3^+). All AuNP were radioactively labeled by neutron irradiation (^{197}Au (n, γ) ^{198}Au) as thoroughly described previously.[5,26,36,37] Physicochemical parameters of the AuNP including specific ^{198}Au radioactivity and the isotope ratio of ^{198}Au to stable ^{197}Au are given in Table 1.

AuNP Administration and Animal Maintenance in Metabolic Cages. The entire administration has been described previously.[5,26] Briefly, the rats were anesthetized by inhalation of 5% isoflurane until muscular tonus relaxed. Each anesthetized rat was fixed with its incisors to a rubber band on a board at an angle of 60° to the lab bench. A flexible cannula (16 G, 2 in) was placed under visual control into the upper third of the trachea. For control of misplacement into the esophagus, exspiration through the cannula was controlled with a pneumotachograph connected to the cannula. The suspension (50 μL) was gently instilled followed by 300−400 μL of air using a 1-mL insulin syringe. Intratracheal instillation was aligned with the rat's inspiration. After administration of the AuNP suspensions, rats were monitored for regular breathing before they were placed individually in metabolic cages for separate collection of urine and feces until dissected at 1, 3, or 24 h postinstillation.

Sample Preparation for Radio Analysis. At different time points postexposure (1, 3, 24 h), rats were anesthetized (5% isoflurane inhalation) and euthanized by exsanguination *via* the abdominal aorta. Approximately 70% of the total blood volume was withdrawn. Radio analysis was performed according to the previous description.[5,26,36,37] Briefly, organs *in toto*, tissues, body fluids, the remaining carcass, and total excretion were sampled and gamma-spectrometrically analyzed as previously described. While dissecting, no organs were cut and all fluids were cannulated, and dissection equipment was regularly changed in order to avoid any cross contamination, when necessary.

The ^{198}Au radioactivity of all samples was measured without any further physicochemical preparation of the samples by gamma-spectroscopy. Small organ and tissue samples were analyzed in a lead-shielded, 10 mL well type NaI(Tl) scintillation detector, while a lead-shielded, 1 L well type NaI(Tl) scintillation detector was used for large samples like the remaining carcass. The count rates were adjusted for physical decay and background radiation. Additionally, count rates were calibrated to a ^{198}Au reference source at a reference date in order to correlate ^{198}Au radioactivity to the numbers, surface areas, and masses of the AuNP. Samples yielding net counts (*i.e.*, background-corrected counts) in the photopeak region-of-interest of the ^{198}Au gamma spectrum were defined to be below the detection limit when they were less than three standard deviations of the background counts of this region-of-interest. By this approach, we quantitatively determined the entire AuNP dose in the entire animal by analyzing each organ and tissue and total excretion in a 100% balance of the biodistribution of the initially applied AuNP dose to the peripheral lungs. The peripheral lung dose (initial dose, ID) was determined by correcting the instilled dose by the fractions in trachea, gastrointestinal tract (GIT), and fecally excreted doses during 24 h, because these rely on mucociliary clearance as discussed in the Results and Discussion section.

Blood Correction in Organs and Adjustment for Mucociliary Clearance. Blood contents of organs and the remaining body were calculated according to the findings of Oeff *et al.*[56] as described previously.[5,26,36,37] The mucociliary clearance (MCC) of AuNP from the thoracic airways toward larynx was considered to contribute negligibly to the ABB translocation. Therefore, the radioactivity measurements of the trachea, gastrointestinal tract (GIT), and head were performed but not included into the complete balance.[26] As previously shown, the fraction of absorbed AuNP through the intestinal barrier is very low and would be only 0.1% for the 18 nm AuNP showing the highest mucociliary cleared AuNP percentage of 57%.[37] Therefore, we did not correct for possible intestinal absorption of maximally 5.7% absorbed AuNP resulting from mucociliary cleared AuNP.

Auxiliary 24-h Biodistribution Studies after Administration of a Soluble ^{198}Au Ion Solution. As described in detail in the Supporting Information, auxiliary 24-h biodistribution studies, after intratracheal instillation of a soluble ^{198}Au ion solution, were performed in order to estimate the possible extent of AuNP dissolution *in vivo*. The ^{198}Au radio-isotope was obtained from neutron irradiation of a $HAuCl_4$ solution in a nuclear research reactor and subsequently diluted, such that 1 μg of soluble Au radio-labeled with 10 kBq ^{198}Au in the 50 μL dose was administered to each animal by intratracheal instillation.

Calculations and Statistical Analysis. All calculated data are given as a percentage of the relevant integral radioactivity of all samples in each animal with the standard error of the mean (SEM). All calculated significances are based on a one-way analysis of variance (ANOVA) followed by a *post hoc* Tukey test. In case of an individual two-group comparison, the unpaired *t* test was used. The criterion for statistical significance was $p \leq 0.05$, if not otherwise stated.

Conflict of Interest: The authors declare no competing financial interest.

Acknowledgment. We thank Carsten Rudolph from Dr. von Hauner Children's Hospital, Ludwig-Maximillians-University of Munich, for his support of the zeta-potential measurements using the Malvern HPPS5001 instrument. We also thank Dr. Dorothea Alber and Gregor Bukalis from the Helmholtz Zentrum in Berlin for performing the neutron activation of our AuNP at the research reactor BER II. The authors appreciate the technical assistance of Sebastian Kaidel and Nadine Senger. This work was partially supported by the German Research Foundation FOR-627, SPP-1313, PA794/11-1 and PAK 56; the EU-FP6 project Particle-Risk (012912 (NEST)); and the EU FP7 projects NeuroNano (NMP4-SL- 2008-214547), ENPRA (NMP4-SL-2009-228789) as well as InLiveTox (NMP-2008-1.3-2 CP-FP 228625-2) and US-NIH Grant HL074022.

Supporting Information Available: AuNP surface modification and radio-labeling by neutron activiation; physicochemical parameters and dose metrics of administered ^{198}AuNP and their radioactive labels; additionally dose metrics of ^{198}Au; mucociliary clearance of AuNP; AuNP concentrations per gram of organ, tissue, or body fluid; AuNP biokinetics: retention of AuNP in organs and tissue after 1, 3, and 24 h after intratracheal instillation; percentages of translocated AuNP (2.8 nm carboxyl- or amino-coated) in secondary organs, tissue, remainder, blood, and urine 24 h after intratracheal instillation. This material is available free of charge *via* the Internet at http://pubs.acs.org.

Note Added after ASAP Publication: This paper was published ASAP on December 30, 2013. Figures 3, 4, and 5 were replaced and the revised version was reposted on January 15, 2014.

REFERENCES AND NOTES

1. Boisselier, E.; Astruc, D. Gold Nanoparticles in Nanomedicine: Preparations, Imaging, Diagnostics, Therapies and Toxicity. *Chem. Soc. Rev.* **2009**, *38*, 1759–1782.
2. Hainfeld, J. F.; Slatkin, D. N.; Focella, T. M.; Smilowitz, H. M. Gold Nanoparticles: A New X-Ray Contrast Agent. *Br. J. Radiol.* **2006**, *79*, 248–253.
3. Arvizo, R.; Bhattacharya, R.; Mukherjee, P. Gold Nanoparticles: Opportunities and Challenges in Nanomedicine. *Expert Opin. Drug Delivery* **2010**, *7*, 753–763.
4. Bhaskar, S.; Tian, F.; Stoeger, T.; Kreyling, W.; de la Fuente, J. M.; Grazu, V.; Borm, P.; Estrada, G.; Ntziachristos, V.; Razansky, D. Multifunctional Nanocarriers for Diagnostics, Drug Delivery and Targeted Treatment across Blood-Brain-Barrier: Perspectives on Tracking and Neuroimaging. *Part. Fibre Toxicol.* **2010**, *7*, 3.
5. Semmler-Behnke, M.; Kreyling, W. G.; Lipka, J.; Fertsch, S.; Wenk, A.; Takenaka, S.; Schmid, G.; Brandau, W. Biodistribution of 1.4- and 18-nm Gold Particles in Rats. *Small* **2008**, *4*, 2108–2111.
6. Dykman, L.; Khlebtsov, N. Gold Nanoparticles in Biomedical Applications: Recent Advances and Perspectives. *Chem. Soc. Rev.* **2012**, *41*, 2256–2282.
7. Ghosh, P.; Han, G.; De, M.; Kim, C. K.; Rotello, V. M. Gold Nanoparticles in Delivery Applications. *Adv. Drug Delivery Rev.* **2008**, *60*, 1307–1315.
8. Mansour, H. M.; Rhee, Y. S.; Wu, X. Nanomedicine in Pulmonary Delivery. *Int. J. Nanomed.* **2009**, *4*, 299–319.
9. Brown, C. L.; Whitehouse, M. W.; Tiekink, E. R.; Bushell, G. R. Colloidal Metallic Gold Is Not Bio-Inert. *Inflammopharmacology* **2008**, *16*, 133–137.
10. De Jong, W. H.; Hagens, W. I.; Krystek, P.; Burger, M. C.; Sips, A. J.; Geertsma, R. E. Particle Size-Dependent Organ Distribution of Gold Nanoparticles after Intravenous Administration. *Biomaterials* **2008**, *29*, 1912–1919.
11. Gosens, I.; Post, J. A.; de la Fonteyne, L. J.; Jansen, E. H.; Geus, J. W.; Cassee, F. R.; de Jong, W. H. Impact of Agglomeration State of Nano- and Submicron Sized Gold Particles on Pulmonary Inflammation. *Part. Fibre Toxicol.* **2010**, *7*, 37.
12. Schulz, M.; Ma-Hock, L.; Chodakowski, K.; Sandra, B.; Wiench, K.; van Ravenzwaay, B.; Hartwig, A.; Landsiedel, R. *In Vitro* and *in Vivo* Studies on the Genotoxicity of Nanomaterials in Lung Tissue. *Naunyn-Schmiedeberg's Arch. Pharmacol.* **2011**, *383*, 14–15.
13. Brandenberger, C.; Rothen-Rutishauser, B.; Muhlfeld, C.; Schmid, O.; Ferron, G. A.; Maier, K. L.; Gehr, P.; Lenz, A. G. Effects and Uptake of Gold Nanoparticles Deposited at the Air-Liquid Interface of a Human Epithelial Airway Model. *Toxicol. Appl. Pharmacol.* **2010**, *242*, 56–65.
14. Sung, J. H.; Ji, J. H.; Park, J. D.; Song, M. Y.; Song, K. S.; Ryu, H. R.; Yoon, J. U.; Jeon, K. S.; Jeong, J.; Han, B. S.; *et al.* Subchronic Inhalation Toxicity of Gold Nanoparticles. *Part. Fibre Toxicol.* **2011**, *8*, 16.
15. Goodman, C. M.; McCusker, C. D.; Yilmaz, T.; Rotello, V. M. Toxicity of Gold Nanoparticles Functionalized with Cationic and Anionic Side Chains. *Bioconjugate Chem.* **2004**, *15*, 897–900.

16. Huhn, D.; Kantner, K.; Geidel, C.; Brandholt, S.; De Cock, I.; Soenen, S. J.; Rivera Gil, P.; Montenegro, J. M.; Braeckmans, K.; Mullen, K.; *et al.* Polymer-Coated Nanoparticles Interacting with Proteins and Cells: Focusing on the Sign of the Net Charge. *ACS Nano* **2013**, *7*, 3253–3263.
17. Chen, Y. S.; Hung, Y. C.; Liau, I.; Huang, G. S. Assessment of the *in Vivo* Toxicity of Gold Nanoparticles. *Nanoscale Res. Lett.* **2009**, *4*, 858–864.
18. Alkilany, A. M.; Murphy, C. J. Toxicity and Cellular Uptake of Gold Nanoparticles: What We Have Learned So Far? *J. Nanopart. Res.* **2010**, *12*, 2313–2333.
19. Khlebtsov, N.; Dykman, L. Biodistribution and Toxicity of Engineered Gold Nanoparticles: A Review of *in Vitro* and *in Vivo* Studies. *Chem. Soc. Rev.* **2011**, *40*, 1647–1671.
20. Pan, Y.; Leifert, A.; Ruau, D.; Neuss, S.; Bornemann, J.; Schmid, G.; Brandau, W.; Simon, U.; Jahnen-Dechent, W. Gold Nanoparticles of Diameter 1.4 nm Trigger Necrosis by Oxidative Stress and Mitochondrial Damage. *Small* **2009**, *5*, 2067–2076.
21. Tsoli, M.; Kuhn, H.; Brandau, W.; Esche, H.; Schmid, G. Cellular Uptake and Toxicity of Au55 Clusters. *Small* **2005**, *1*, 841–844.
22. Leifert, A.; Pan, Y.; Kinkeldey, A.; Schiefer, F.; Setzler, J.; Scheel, O.; Lichtenbeld, H.; Schmid, G.; Wenzel, W.; Jahnen-Dechent, W.; *et al.* Differential hERG Ion Channel Activity of Ultrasmall Gold Nanoparticles. *Proc. Natl. Acad. Sci. U. S. A.* **2013**, *110*, 8004–8009.
23. Gehr, P.; Bachofen, M.; Weibel, E. R. The Normal Human Lung: Ultrastructure and Morphometric Estimation of Diffusion Capacity. *Respir. Physiol.* **1978**, *32*, 121–140.
24. Yu, L. E.; Lanry Yung, L.-Y.; Ong, C.-N.; Tan, Y.-L.; Suresh Balasubramaniam, K.; Hartono, D.; Shui, G.; Wenk, M. R.; Ong, W.-Y. Translocation and Effects of Gold Nanoparticles after Inhalation Exposure in Rats. *Nanotoxicology* **2007**, *1*, 235–242.
25. Sadauskas, E.; Jacobsen, N. R.; Danscher, G.; Stoltenberg, M.; Vogel, U.; Larsen, A.; Kreyling, W.; Wallin, H. Biodistribution of Gold Nanoparticles in Mouse Lung Following Intratracheal Instillation. *Chem. Cent. J.* **2009**, *3*, 16.
26. Lipka, J.; Semmler-Behnke, M.; Sperling, R. A.; Wenk, A.; Takenaka, S.; Schleh, C.; Kissel, T.; Parak, W. J.; Kreyling, W. G. Biodistribution of PEG-Modified Gold Nanoparticles Following Intratracheal Instillation and Intravenous Injection. *Biomaterials* **2010**, *31*, 6574–6581.
27. Patrick, G.; Stirling, C. Transport of Particles of Colloidal Gold within and from Rat Lung after Local Deposition by Alveolar Microinjection. *Environ. Health Perspect.* **1992**, *97*, 47–51.
28. Takenaka, S.; Karg, E.; Kreyling, W. G.; Lentner, B.; Moller, W.; Behnke-Semmler, M.; Jennen, L.; Walch, A.; Michalke, B.; Schramel, P.; *et al.* Distribution Pattern of Inhaled Ultrafine Gold Particles in the Rat Lung. *Inhalation Toxicol.* **2006**, *18*, 733–740.
29. Takenaka, S.; Moller, W.; Semmler-Behnke, M.; Karg, E.; Wenk, A.; Schmid, O.; Stoeger, T.; Jennen, L.; Aichler, M.; Walch, A.; *et al.* Efficient Internalization and Intracellular Translocation of Inhaled Gold Nanoparticles in Rat Alveolar Macrophages. *Nanomedicine (London, U. K.)* **2012**, *7*, 855–865.
30. Schleh, C.; Holzwarth, U.; Hirn, S.; Wenk, A.; Simonelli, F.; Schaffler, M.; Moller, W.; Gibson, N.; Kreyling, W. G. Biodistribution of Inhaled Gold Nanoparticles in Mice and the Influence of Surfactant Protein D. *J. Aerosol Med. Pulm. Drug Delivery* **2013**, *26*, 24–30.
31. Muhlfeld, C.; Gehr, P.; Rothen-Rutishauser, B. Translocation and Cellular Entering Mechanisms of Nanoparticles in the Respiratory Tract. *Swiss Med. Wkly.* **2008**, *138*, 387–391.
32. Semmler-Behnke, M.; Takenaka, S.; Fertsch, S.; Wenk, A.; Seitz, J.; Mayer, P.; Oberdorster, G.; Kreyling, W. G. Efficient Elimination of Inhaled Nanoparticles from the Alveolar Region: Evidence for Interstitial Uptake and Subsequent Reentrainment onto Airways Epithelium. *Environ. Health Perspect.* **2007**, *115*, 728–733.
33. Kreyling, W. G.; Semmler-Behnke, M.; Takenaka, S.; Moller, W. Differences in the Biokinetics of Inhaled Nano- *Versus* Micrometer-Sized Particles. *Acc. Chem. Res.* **2012**, *46*, 714–722.
34. Chithrani, B. D.; Chan, W. C. Elucidating the Mechanism of Cellular Uptake and Removal of Protein-Coated Gold Nanoparticles of Different Sizes and Shapes. *Nano Lett.* **2007**, *7*, 1542–1550.
35. Chithrani, D. B. Intracellular Uptake, Transport and Processing of Gold Nanostructures. *Mol. Membr. Biol.* **2010**, *27*, 299–311.
36. Hirn, S.; Semmler-Behnke, M.; Schleh, C.; Wenk, A.; Lipka, J.; Schaffler, M.; Takenaka, S.; Moller, W.; Schmid, G.; Simon, U.; *et al.* Particle Size-Dependent and Surface Charge-Dependent Biodistribution of Gold Nanoparticles after Intravenous Administration. *Eur. J. Pharm. Biopharm.* **2011**, *77*, 407–416.
37. Schleh, C.; Semmler-Behnke, M.; Lipka, J.; Wenk, A.; Hirn, S.; Schaffler, M.; Schmid, G.; Simon, U.; Kreyling, W. G. Size and Surface Charge of Gold Nanoparticles Determine Absorption across Intestinal Barriers and Accumulation in Secondary Target Organs after Oral Administration. *Nanotoxicology* **2012**, *6*, 36–46.
38. Pan, Y.; Neuss, S.; Leifert, A.; Fischler, M.; Wen, F.; Simon, U.; Schmid, G.; Brandau, W.; Jahnen-Dechent, W. Size-Dependent Cytotoxicity of Gold Nanoparticles. *Small* **2007**, *3*, 1941–1949.
39. Pellegrino, T.; Sperling, R. A.; Alivisatos, A. P.; Parak, W. J. Gel Electrophoresis of Gold-DNA Nanoconjugates. *J. Biomed. Biotechnol.* **2007**, *2007*, 26796.
40. Rivera-Gil, P.; Jimenez De Aberasturi, D.; Wulf, V.; Pelaz, B.; Del Pino, P.; Zhao, Y.; De La Fuente, J. M.; Ruiz De Larramendi, I.; Rojo, T.; Liang, X.-J.; *et al.* The Challenge to Relate the Physicochemical Properties of Colloidal Nanoparticles to Their Cytotoxicity. *Acc. Chem. Res.* **2013**, *46*, 743–749.
41. Lundqvist, M.; Stigler, J.; Elia, G.; Lynch, I.; Cedervall, T.; Dawson, K. A. Nanoparticle Size and Surface Properties Determine the Protein Corona with Possible Implications for Biological Impacts. *Proc. Natl. Acad. Sci. U. S. A.* **2008**, *105*, 14265–14270.
42. Lundqvist, M.; Stigler, J.; Cedervall, T.; Berggard, T.; Flanagan, M. B.; Lynch, I.; Elia, G.; Dawson, K. The Evolution of the Protein Corona around Nanoparticles: A Test Study. *ACS Nano* **2011**, *5*, 7503–7509.
43. Patrick, G.; Stirling, C. Slow Clearance of Different-Sized Particles from Rat Trachea. *J. Aerosol Med.* **1997**, *10*, 55–65.
44. Conner, S. D.; Schmid, S. L. Regulated Portals of Entry into the Cell. *Nature* **2003**, *422*, 37–44.
45. Rejman, J.; Oberle, V.; Zuhorn, I. S.; Hoekstra, D. Size-Dependent Internalization of Particles *Via* the Pathways of Clathrin- and Caveolae-Mediated Endocytosis. *Biochem. J.* **2004**, *377*, 159–169.
46. Semmler, M.; Seitz, J.; Erbe, F.; Mayer, P.; Heyder, J.; Oberdorster, G.; Kreyling, W. G. Long-Term Clearance Kinetics of Inhaled Ultrafine Insoluble Iridium Particles from the Rat Lung, Including Transient Translocation into Secondary Organs. *Inhalation Toxicol.* **2004**, *16*, 453–459.
47. Kreyling, W. G.; Semmler-Behnke, M.; Seitz, J.; Scymczak, W.; Wenk, A.; Mayer, P.; Takenaka, S.; Oberdorster, G. Size Dependence of the Translocation of Inhaled Iridium and Carbon Nanoparticle Aggregates from the Lung of Rats to the Blood and Secondary Target Organs. *Inhalation Toxicol.* **2009**, *21*, 55–60.
48. Papasani, M. R.; Wang, G.; Hill, R. A. Gold Nanoparticles: The Importance of Physiological Principles to Devise Strategies for Targeted Drug Delivery. *Nanomedicine (London, U. K.)* **2012**, *8*, 804–814.
49. Choi, H. S.; Liu, W.; Misra, P.; Tanaka, E.; Zimmer, J. P.; Ipe, B. I.; Bawendi, M. G.; Frangioni, J. V. Renal Clearance of Quantum Dots. *Nat. Biotechnol.* **2007**, *25*, 1165–1170.
50. Schäffler, M.; Semmler-Behnke, M.; Sarioglu, H.; Takenaka, S.; Wenk, A.; Schleh, C.; Hauck, S. M.; Johnston, B. D.; Kreyling, W. G. Serum Protein Identification and Quantification of the Corona of 5, 15 and 80 nm Gold Nanoparticles. *Nanotechnology* **2013**, *24*, 265103.

51. Johnsson, E.; Haraldsson, B. Addition of Purified Orosomucoid Preserves the Glomerular Permeability for Albumin in Isolated Perfused Rat Kidneys. *Acta Physiol. Scand.* **1993**, *147*, 1–8.
52. Rodewald, R.; Karnovsky, M. J. Porous Substructure of the Glomerular Slit Diaphragm in the Rat and Mouse. *J. Cell Biol.* **1974**, *60*, 423–433.
53. Haraldsson, B.; Nystrom, J.; Deen, W. M. Properties of the Glomerular Barrier and Mechanisms of Proteinuria. *Physiol. Rev.* **2008**, *88*, 451–487.
54. Chithrani, D. B.; Dunne, M.; Stewart, J.; Allen, C.; Jaffray, D. A. Cellular Uptake and Transport of Gold Nanoparticles Incorporated in a Liposomal Carrier. *Nanomedicine (London, U. K.)* **2010**, *6*, 161–169.
55. Deen, W. M.; Lazzara, M. J.; Myers, B. D. Structural Determinants of Glomerular Permeability. *Am. J. Physiol.: Renal, Fluid Electrolyte Physiol* **2001**, *281*, F579–596.
56. Oeff, K.; Konig, A. Blood Volume of Rat Organs and Residual Amount of Blood after Blood Letting or Irrigation; Determination with Radiophosphorus-Labeled Erythrocytes. *Naunyn-Schmiedeberg's Arch. Exp. Pathol. Pharmakol.* **1955**, *226*, 98–102.
57. Turkevich, J.; Stevenson, P. C.; Hilliery, J. A Study of the Nucleation and Growth Processes in the Synthesis of Colloidal Gold. *Discuss. Faraday Soc.* **1951**, 55–75.
58. Tominaga, T.; Tenma, S.; Watanabe, H.; Giebel, U.; Schmid, G. Tracer Diffusion of a Ligand-Stabilized Two-Shell Gold Cluster. *Chem. Lett.* **1996**, *25*, 1033–1034.